

Design of photoelectrochemical detection of miRNA-221 based on tungsten diselenide-cysteine-dopamine nanoprobe coupled with mismatch catalytic hairpin assembly target recycling with ultralow background noise

Ting Yao ^a, Xu Hun ^{a*}

S1. Experimental section

S1.1 Chemicals and reagents

Bulk WSe₂ was obtained from J&K Scientific Ltd (Beijing, China). 1,2-dichlorobenzene (DCB) were purchased from Tianjin Guangcheng Reagent Company (Tianjin, China). Tris-(hydroxymethyl) aminomethane (Tris), Tris-EDTA buffer solution (TE buffer), Tris-acetate-EDTA buffer solution (TAE buffer), N-Hydroxysuccinimide (NHS), 1-Ethyl-3-(3-dimethylaminopropyl) carbodiimide hydrochloride (EDC) and 6-mercaptohexanol (MCH) were ordered from Sangon Biotech Co. Ltd. (Shanghai, China), and the DNA and RNA base sequences were listed in **Table S1**. All the other reagents were obtained from Aladdin (Shanghai, China). The chemical reagents used in our experiment were of analytical grade and were used as received without further purification. All aqueous solutions were prepared using ultrapure water from an Aquapro Ultrapure Water System (Ever Young Enterprises Development. Co., Ltd., Chongqing, China).

Table S1. Sequence information of the nucleic acids

Name	Sequences (from 5' to 3')
H1	GTC TGC TGG GTT TCG CGT AAC GTA TGA AAC CCA GCA GAC AAT GTA GCT-SH
H2	GTA ACG TAT GAA ACC CAT TGT CTG CTG GGT TTC ATA CGT TAC GCG AAA CCC-SH
miRNA-221	AGC UAC AUU GUC UGC UGG GUU UC
one-base mismatch I	AGC UAC <u>T</u> UU GUC UGC UGG GUU UC
one-base mismatch II	AGC UAC AUU GUC <u>U</u> CC UGGGUU UC
two-base mismatch	AGC UAC <u>T</u> UU GUC <u>U</u> CC UGG GUU UC
let-7a	UGA GGU AGU AGG UUG UAU AGU U
miRNA-155	UUA AUG CUA AUC GUG AUA GGG GU
miRNA-141	UAA CAC UGU CUG GUA AAG AUG G

S1.2 Apparatus

The surface morphology of bulk WSe₂ and exfoliated WSe₂ was observed via scanning electron microscopy (SEM, JSM-6700F, Japan) and transmission electron microscopy (TEM, JEM-2100, USA). The prepared nanoprobe of infrared spectra was recorded on a Nicolet NEXUS870 Fourier transform infrared (FT-IR) spectrometer (Madison, WI). Photocurrent was performed on a CHI 660E electrochemical working station (CHI instrument, USA) with a conventional three-electrode cell. A gold electrode (GE) or modified gold electrode was used as the working electrode, saturated calomel electrode (SCE) as reference electrode and a platinum wire as counter electrode. Time profiles of OCP were measured in phosphate buffer under dark and illuminated conditions. The electrochemical characterization was executed by EIS in 5.0 mM [Fe(CN)₆]^{3-/4-} solution, at a direct current potential of 0.2 V. A Molecular Imager Gel Doc XR+ with Image Lab software (Bio-Rad, California, USA) was employed for the gel electrophoresis image.

S1.3 Exfoliation of WSe₂

In ultrasonic exfoliation process, DCB has been shown to have auxiliary

function¹. First, 1.0 g commercially available WSe₂ powder was dispersed in 100 mL DCB. After sonication for 10 h in 0 °C ice-water bath, large particles were removed by centrifugation at 1700 rpm for 3 min. Then the product was treated as previously described method². DCB was removed from the dispersion by several centrifugation wash cycles with chloroform. The exfoliated WSe₂ was used as photoactive material.

S1.4 Preparation of nanoprobe

First, 0.24 g Cys and 0.06 g exfoliated WSe₂ was added to 2 mL absolute ethanol and then sonicated for 12 h at room temperature³⁻⁵. Whereafter, the mixed liquor was centrifuged at 15,000 rpm for 30 min to remove unattached Cys. Subsequently, 100 μL 20 mg mL⁻¹ EDC was added into the mixture to activate the carboxyl and 25 μL 20 mg mL⁻¹ NHS were added to improve reaction efficiency at room temperature⁶. Ultimately, 0.015 g DA was added to the obtained WSe₂/Cys mixture, simultaneously stirring for 16 h under dark seal conditions to obtain the nanoprobe via amidation reaction⁷. The prepared nanoprobe, WSe₂/Cys/DA, centrifuged for 30 min at 12,000 rpm and washed three times with ethanol to remove the free DA. Then the obtained WSe₂/Cys/DA was diluted to 2 mL with 1×TAE buffer solution and stored in brown glass bottles at 4 °C.

S1.5 Preparation of PEC probe

Two hairpin DNA segments, H1 and H2, were employed in the mmCHA process, each hairpin DNA was heated to 95 °C for 5 min and then allowed to cool to room temperature for at least 2 h. The 10 μL of 10 μM thioled H2 was added into 100 μL WSe₂/Cys/DA, and then incubated for 5 h in constant temperature oscillator under 120 rpm at room temperature, resulting H2 attach to WSe₂ via a thiol group. Whereafter, the mixed liquor was centrifuged at 12,000 rpm for 30 min to remove unattached DNA. The PEC probe, H2/WSe₂/Cys/DA, was obtained.

S1.6 Fabrication of PEC biosensor

The principle of miRNA biosensor fabrication was illustrated in **Scheme 1**. Initially, in order to assemble the numerous H1, the GE was immersed in 0.1% HAuCl₄ solution at a constant potential of -0.2 V for 400 s for electrochemical deposition to gain AuNPs modified electrode, namely, AuNPs/GE. Apart from the large specific surface area, the good conductivity of AuNPs can accelerate electron transfer⁸. Certain amount of thioled H1 was added into 1×TAE buffer solution. Then, 20 μL of 1 μM H1 solution was dropped onto the surface of the AuNPs/GE for one night at room temperature, after that, the electrode was thoroughly washed with Tris-HCl buffer (pH = 7.4, 10 mM) to remove the unattached DNA. Next, the electrode was immersed into 1 mM MCH to block the unbound sites. After that, the electrode was rinsed with Tris-HCl buffer. Finally, the modified electrode was immersed into 50 μL Tris-HCl solution contained 30 μL different concentration of miRNA-221 and 20 μL H2/WSe₂/Cys/DA simultaneously and incubated at 37 °C for 90 min. When the assembly finished, the resulting electrode was rinsed thoroughly for testing.

S1.7 PEC measurement

The PEC biosensor was investigated in 0.1 M phosphate buffer solution (pH 7.4) irradiated with 10 W LED lamp. The light was switched off-on-off for 10 s - 10 s - 10 s under -0.2 V potential.

S1.8 Gel electrophoresis

The polyacrylamide gel electrophoresis (PAGE) was carried out to characterize the functioning process of target-triggered mismatch catalytic hairpin (mmCHA) in our experiment. Briefly, H1 (10 μ L), target (10 μ L), H2 (10 μ L), a mixture of H1 and target (10 μ L), a mixture of H1, target and H2 (10 μ L), a mixture of H1 and H2 (10 μ L) were mixed with 6 \times loading buffer solution (2 μ L), respectively. Next, these samples were subjected to the polyacrylamide gel (16 %), followed by conducting in 1 \times TE buffer at 135 V for 80 min. Finally, the gels were stained with ethidium bromide (EB) for 15 min, followed by recorded through a Molecular Imager Gel Doc XR+ with Image Lab software.

S1.9 Control experimental

S1.9.1 Preparation of modified GE

Prior to surface modification, the GE was polished with alumina slurry, followed by sonicating in ultrapure water and anhydrous ethanol. The well-polished bare GE was first immersed in HAuCl₄ solution as above to gain AuNPs/GE (S1.6). After dried in air, AuNPs/GE coated with exfoliated WSe₂ dispersion (15 μ L, 2 mg mL⁻¹) to gain WSe₂/AuNPs/GE.

S1.9.2 Preparation of DNA probe

In the control experiment, amidation reaction of DA with COOH groups at Cys is carried out. Then, Cys/DA is assembled onto H2 by disulfide bond⁹. The resulting DNA probe was abbreviated as H2/Cys/DA.

S1.9.3 Fabrication of PEC biosensor of Method A

As the previous experiment details of S1.6, firstly, 20 μ L of 1 μ M H1 solution was dropped onto the surface of the WSe₂/AuNPs/GE for one night. After blocked by MCH solution for 1 h, the H1/WSe₂/AuNPs/GE was hybridized with different concentration of miRNA and H2/Cys/DA and incubated at 37 $^{\circ}$ C for 90 min. When the assembly finished, the resulting electrode was rinsed thoroughly for tested.

S1.10 Preparation of real samples

S1.10.1 Preparation of human serum

To evaluate the applicability of this PEC biosensor for the detection of miRNA-221 in real samples, we employed the healthy human serum (provided by the Qingdao Center Hospital, China) as the sample matrixes to test miRNA-221 via standard addition method. The human real serum samples were isolated from the whole blood by the centrifugation at 3000 rpm for 20 min and the supernatant kept frozen at -20 $^{\circ}$ C. Then, the resulting human serum sample was first treated with an RNase inhibitor to prevent miRNA degradation¹⁰. Different concentrations of miRNA-221 (0.0, 5.0 pM, 10.0 pM, 50.0 pM, 100.0 pM) were added into serum sample 10-fold diluted with Tris-HCl buffer and detected by the developed PEC biosensor.

S1.10.2 Cell culture and total RNA extraction

Human cancer cell lines including human cervical cancer cell (HeLa) and human embryonic kidney cell line (HEK293T cells) were purchased from Cell Bank of Chinese Academy of Sciences (Shanghai, China). HeLa and HEK293T cells were cultured in a humidified atmosphere with 5% CO₂ under 37 $^{\circ}$ C, using RPMI 1640 medium with 10% fetal bovine serum. All of the cells were resuspended and collected

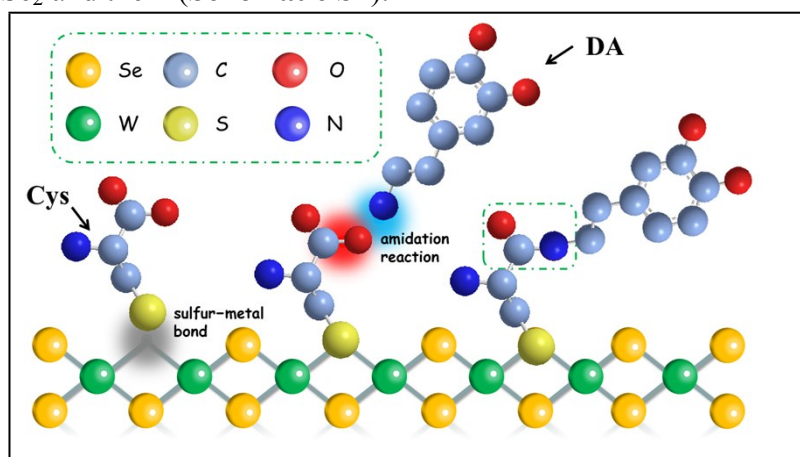
resuspended by fresh medium and trypsinization, respectively. HeLa and HEK293T extracts were treated by the SanPrep Column microRNA Mini-Preps Kit (Sangon Biotech, Shanghai), and stored at -20 °C before use. The endogenous miR-221 levels are detected by measuring 10 ng of total RNA extracted from HEK293T cells and HeLa cells with this PEC biosensor, respectively. To improve the accuracy of the results, 0 ng of total RNA is considered as the control group.

For qRT-PCR assay, the total RNA was quantified by using the Mir-X™ miRNA qRT-PCR SYBR Kit (TaKaRa, Dalian, China) following the recommended procedures of the manufacture. The qRT-PCR^{11, 12} was employed and performed in a BIO-RAD CFX connect Real-Time system (Singapore), and the calibration curve between Ct values and the logarithm (log) of miRNA-221 concentrations was obtained by using synthetic standard miRNA-221. Finally, the concentration of miRNA-221 in 10 ng total RNA extract was calculated according to the calibration curve.

S2. Results and discussions

S2.1 The schematic of nanoprobe preparation

Due to ultrasonic cavitation and sufficient acoustic shearing¹³, the prepared exfoliated WSe₂ can produce selenium defects at the peripheral edges and vacancies in internal of WSe₂^{14, 15}. According to the literature, sulfur functional groups can be bonded with WSe₂ via sulfur-metal bond^{14, 16, 17}. Accordingly, in this work, we have modified WSe₂ surfaces with thiol-capping reagents Cys, thus forming amine-functionalized WSe₂ (WSe₂/Cys). Then the electron donor DA can be assembled onto the WSe₂/Cys via amidation reaction with -COOH of Cys⁷, the resulting probe was abbreviated as WSe₂/Cys/DA. Cys and DA attached on WSe₂ enable charge transfer between WSe₂ and them (**Schematic S1**).



Schematic S1. Schematic illustration of probe preparation with sulfur-metal bond and carbodiimide method

S2.2 Morphology characterization of bulk WSe₂

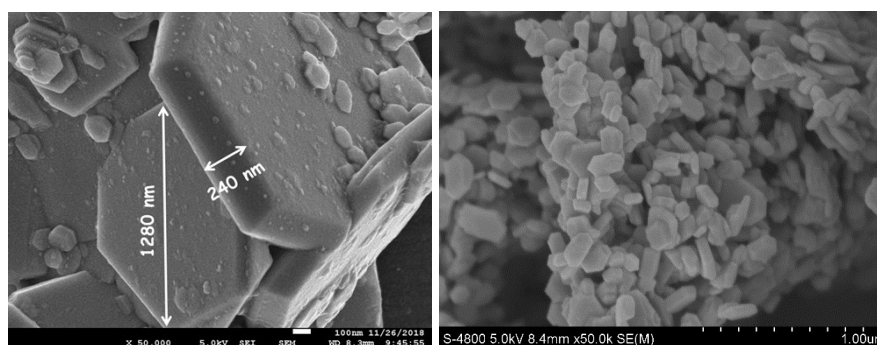


Fig. S1 SEM images of bulk WSe₂ (A) and exfoliated WSe₂ (B).

The morphology of bulk WSe₂ and exfoliated WSe₂ is shown in **Fig. S1**. The bulk WSe₂ is shown in **Fig. S1 (A)**. The bulk WSe₂ has lateral dimensions of 1280 ± 65 nm, exhibiting irregular hexagonal shapes, and the thickness is around 240 ± 18 nm. After exfoliation, the WSe₂ became thinner and smaller. With the reduction of size, the thickness is decreased to about 31 ± 3 nm and lateral flake size of about 200 ± 12 nm (**Fig. S1 (B)**, **Fig. 1 (A)**, **(B)**).

S2.3 PEC response of bulk WSe₂ and exfoliated WSe₂

In order to compare the PEC properties of exfoliated material with the bulk material, 15 μ L of exfoliated WSe₂ and bulk WSe₂ were respectively modified the GE, and the phosphate buffer or phosphate buffer contained 0.1 mM DA as detection solution. The results are shown in **Fig. S2 (A)**. In the absence of DA the bulk WSe₂ modified GE (cure a) and exfoliated WSe₂ modified GE (cure c) has no obvious photocurrent response, but curve c (17.5 nA) is lightly higher than curve a (8.3 nA). In the presence of DA, the photocurrent response of exfoliated WSe₂ modified GE (2014.5 nA, cure d) showed PEC signal about 3.3 folds compared with that of bulk WSe₂ modified GE (604.3 nA, cure b). This indicates that exfoliated WSe₂ has higher optoelectronic activity, can efficiently enhance the photocurrent response. So subsequent PEC biosensor is constructed with exfoliated WSe₂.

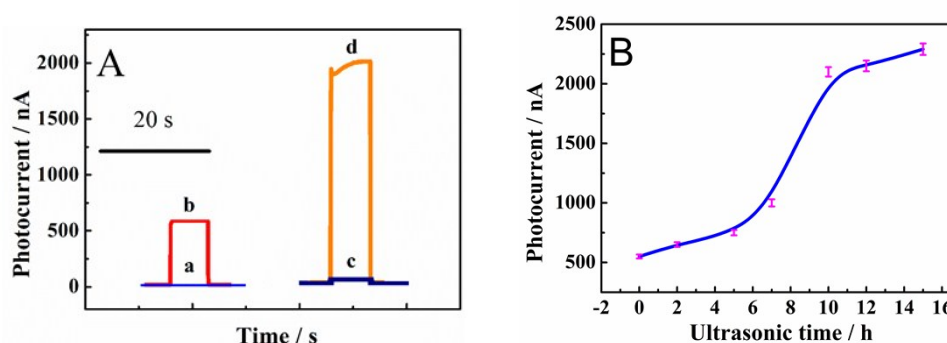


Fig. S2 (A) The PEC response of bulk WSe₂ modified GE in phosphate buffer in the presence of (b) and absence of (a) 0.1 mM DA; exfoliated WSe₂ modified GE in phosphate buffer in the presence of (d) and absence of (c) 0.1 mM DA. **(B)** Effect of ultrasonic time of WSe₂ on the PEC response.

Furthermore, the effect of the ultrasonic time of WSe₂ on the PEC response was evaluated. As shown in **Fig. S2 (B)**, the peak current increases when the time ranges from 7 to 10 h, and almost remains stable after 10 h. Thus, 10 h of ultrasonic time was used.

S2.4 Screening of electron donors

As a PEC detection protocol, electron donors are very important. So many small molecules were tested to select the ideal electron donors. These substances including DA, Cys, Ascorbic Acid (AA). et. al, were respectively added into the detection solution (10 μM). The photocurrent intensity of WSe₂/GE was recorded. As shown in **Fig. S3**, a doughty enhancement of photocurrent was generated only when DA acts as an electron donor. While Cys was presented, the photocurrent increases slightly. The reason may be that DA and Cys were powerful reducing amino acid, which can effectively suppressed the recombination of the WSe₂ photo-generated electrons and holes^{18, 19}. Thus, DA was chosen as the electron donor for subsequent experiment. Furthermore, Cys can be an admirable linker when DA is modified on WSe₂. This Cys-linking strategy could generate the synergistic effect to ultimately achieve the goal that enhance the photocurrent response in dection system.

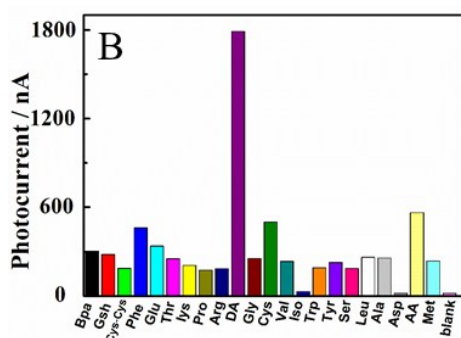


Fig. S3 The PEC response of different small molecules to WSe₂/GE.

S2.5 FT-IR spectra of nanoprobe

Fig. 1 (D) shows FT-IR spectra of Cys, WSe₂/Cys and WSe₂/Cys/DA. The characteristic absorption peaks of Cys were observed at 1617 cm⁻¹, 3049 cm⁻¹, 3346 cm⁻¹ ~ 3232 cm⁻¹, 1298 cm⁻¹, 2639 cm⁻¹, 813 cm⁻¹, which can be corresponded to the bending vibration of C=O, stretching vibration of O-H, stretching vibration of NH₂, out-of-plane wagging vibration of CH₂, stretching vibration of S-H, typical vibration of C-S. From the IR spectra of WSe₂/Cys, the typical peaks of S-H at 2639 cm⁻¹ disappeared due to the coordination of the thiol group of Cys with the metal ions on the surface, and other characteristic absorption peaks shifted in different degrees, indicating that Cys was modified on the surface of WSe₂. Besides these adsorption peaks derived from WSe₂/Cys, WSe₂/Cys/DA showed some additional peaks at 1695 cm⁻¹ and 3380 cm⁻¹ correspond to the bending vibration of C=O, stretching vibration of amide N-H, while 1607 cm⁻¹ - 1577 cm⁻¹ and 1315 cm⁻¹ can attributed to the benzene ring skeleton and bending vibration of phenolic O-H²⁰⁻²². Moreover, C-N and C-H of DA in the 1218 cm⁻¹ and 3009 cm⁻¹ peak were also observed, respectively, which further illustrated this nanoprobe, WSe₂/Cys/DA, is successful prepared.

S2.6 The functioning process of mmCHA characterized by Gel electrophoresis

The polyacrylamide gel electrophoresis was executed to confirm the functioning process of mmCHA. As shown in **Fig. 3(A)**, for the H1 (lane 1) and H2 (lane 3) was observed with a much lower migration rate than the target strand (lane 2), because single strand DNA with different molecular weight could lead to different migration. The result of H1 incubated with target was shown in lane 3, which presented a slower band shift compared with lane 1, 2, indicating that the hybridization between H1 and target was successful. After H2 was incubated with H1 and target for 1 h (Lane 5), a band migration with the slowest mobility was obviously observed, and the weak band of H1 incubated with target had almost disappeared suggesting the successful generation of mmCHA. Additionally, the H1+H2 mixture (lane 6) showed no change of their corresponding bands, indicating that H1 and H2 cannot open spontaneously and product duplex DNA chain.

S2.7 Optimization of experimental conditions

To achieve an optimal analytical performance of the PEC biosensor, several experimental conditions were investigated. As a PEC detection protocol, we screened the potential and the pH of the detection solution that may affect the PEC signal. We selected $-0.3\text{ V} \sim 0.3\text{ V}$ as the experiment potential. Here, the difference (ΔI) between signal value (I) and blank value (I_0) and the ratio (I/I_0) of signal value to blank value were used as the standards. The photocurrent intensity of the resulting electrodes H2/WSe₂/Cys/DA/miRNA/MCH/H1/AuNPs/GE was recorded in 0.1 M phosphate buffer (pH 7.4) irradiated with a LED. **Fig. S4 (A)** shows the photocurrent of I and I_0 in different test potential. **Fig. S4 (B)** displays that ΔI at 0.3 V was larger than that at -0.2 V , but the ratio at 0.3V was far lower than that at -0.2 V , so -0.2 V was selected as the optimal potential for subsequent experiment. Similarly, as shown in **Fig. S4 (C, D)**, when the pH of the detection solution was 7.5, the ΔI raised to the maximum value nearly about 491.2 nA, this consistent with the result of I/I_0 . So, 7.5 was chosen as the ideal pH for the following studies.

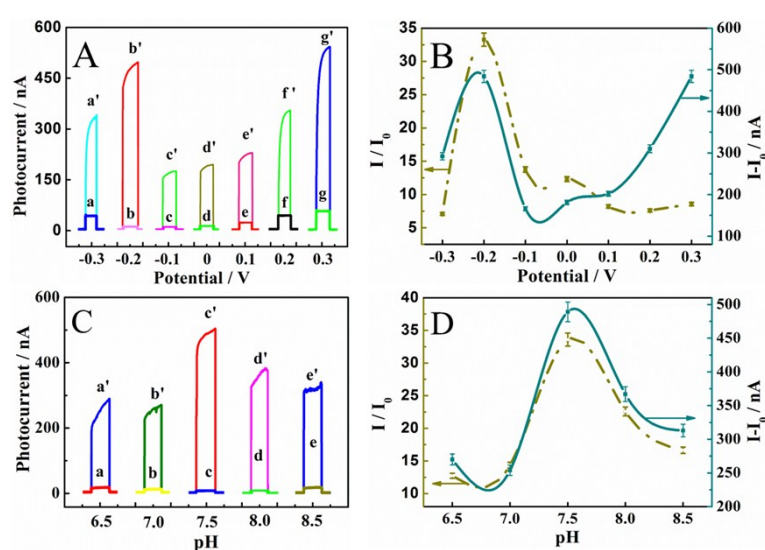


Fig. S4 The influence of potential (A and B) and pH of the phosphate buffer (C and D) on the photocurrent responses. PEC detection performed with miRNA marked up

with superscript and lower case letter (I) and without miRNA marked up with lower case letter (I_0). The difference ($\Delta I = I - I_0$) indicated by a solid line while the ratio (I/I_0) shown by a dotted line. The concentration of miRNA was 1 nM.

S2.8 Analytical performance of PEC biosensor

To investigate the quantitatively analytical performance of this PEC biosensor, PEC measurements were taken under the optimal experiment conditions. **Fig. S5 (A)** depicted the PEC responses continuously increased with increasing concentration of miRNA-221 from 0.1 fM to 1.0 nM. There was a good linear relationship between the photocurrent and the logarithmic value of miRNA concentrations (**Fig. S5 (B)**). The equation of linear regression was $I = 51.31 \log C(M) + 955.4$ ($R^2 = 0.9995$) where I, C, and R represented the PEC signal value, the miRNA-221 concentration and the correlation coefficient, respectively. Furthermore, the sensitivity of this biosensor was compared with previously reported strategies as performed in **Table 1**.

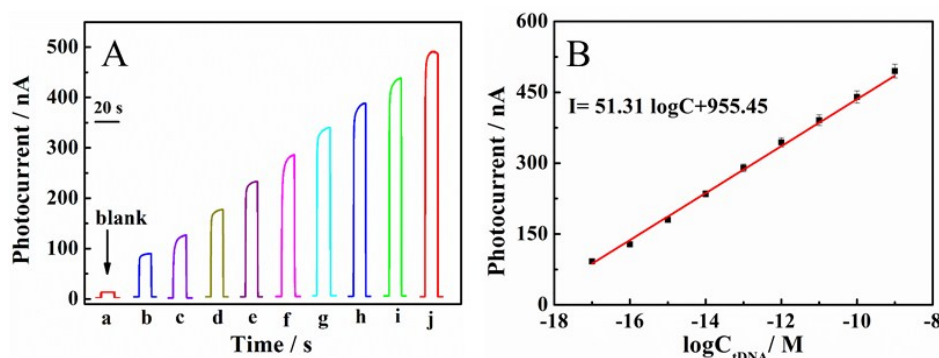


Fig. S5 (A) PEC responses of the biosensor incubated with different miRNA-221 concentrations: 0.0 aM, 10.0 aM, 100.0 aM, 1.0 fM, 10.0 fM, 100.0 fM, 1.0 pM, 10.0 pM, 100.0 pM and 1.0 nM (from a to j). (B) The corresponding linear calibration plot for miRNA-221 detection.

S2.9 Specificity of PEC biosensor

The specificity of this biosensor was investigated by employing several interfering agents, including miRNA-155, miRNA-141, let-7a, and thrombin were assessed as controls. As shown in **Fig. S6 (A)**, the PEC response of the blank test exhibited no difference in comparison with 10.0 nM miRNA-155, 10.0 nM miRNA-141, 10.0 nM let-7a and 10.0 nM thrombin. While 100.0 pM miRNA-221 was used as the detection sample, a significantly increased PEC response was observed. In addition, the mixture containing 10 nM miRNA-155, 10.0 nM miRNA-141, 10.0 nM let-7a, 10.0 nM thrombin and 100.0 pM miRNA-221 exhibited no obvious variation in PEC response compared with that of individually miRNA-221. Consequently, the results suggested that this PEC biosensor showed a good selectivity towards miRNA-221 assay.

In order to further show the specificity of the sensor, the PEC biosensor was evaluated via homologous miRNA sequences involving miRNA-221, one-base mismatch RNA at different locations, two-base mismatch RNA under the LOD concentration. One method, homologous miRNA sequences, target miRNA, and their

mixtures, were detected at LOD concentrations (3.3 aM), respectively. The results are added in **Fig. S6 (B)**. The other method, 3.3 aM target miRNA, 33.0 aM homologous miRNA sequences and their mixtures at the same concentration were also detected. The results are added in **Fig. S6 (C)**. It can obviously gain that this PEC biosensor has well selectivity to target miRNA-221.

S2.10 Stability of PEC biosensor

The stability of the PEC biosensor was assessed via incubated with 100 pM miRNA-221 and monitored under successive periodic “off–on–off” light for 5 cycles. As illustrated in **Fig. S6 (D)**, the relative standard deviation (RSD) for photocurrent responses was 3.2%. After the sensing electrode being stored in a dark and humid condition at 4 °C for a month, the PEC responses of the modified electrodes remained at 96.1% of its original value. As illustrated in **Fig. S6 (E)**, which indicated the biosensor was possessed of an excellent stability along with a satisfied RSD.

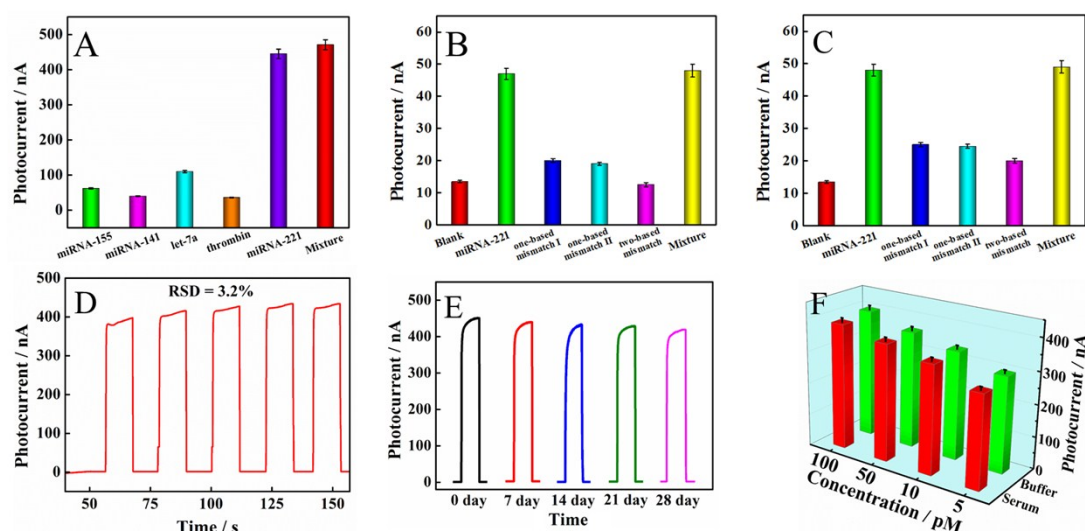


Fig. S6 Selectivity of the PEC biosensor with various targets: (A) 10.0 nM miRNA-155, 10.0 nM miRNA-141, 10.0 nM let-7a and 10.0 nM thrombin, 100.0 pM miRNA-221, and the mixture containing 10.0 nM miRNA-155, 10.0 nM miRNA-221, 10.0 nM let-7a and 10.0 nM thrombin, 100.0 pM miRNA-221. (B) miRNA-221 (3.3 aM), one-base mismatch I (3.3 aM), one-base mismatch II (3.3 aM), two-base mismatch (3.3 aM), and the mixture. The mixture containing 3.3 aM miRNA-221, 3.3 aM one-base mismatch I, 3.3 aM one-base mismatch II, 3.3 aM two-base mismatch. (C) miRNA-221 (3.3 aM), one-base mismatch I (33 aM), one-base mismatch II (33 aM), two-base mismatch (33 aM), and the mixture. The mixture containing 3.3 aM miRNA-221, 33 aM one-base mismatch I, 33 aM one-base mismatch II, 33 aM two-base mismatch. (D) Time-based photocurrent responses of the PEC biosensor under periodic off–on–off light for 5 cycles. (E) Stability of the PEC biosensor for a month of storage. (F) The PEC response of biosensor at different concentrations of miRNA-221 in real serum sample and phosphate buffer.

S2.11 Detection of miRNA-221 in human serum samples

Table S2 Results of determination of miRNA-221 in human serum.

Sample ^a	Added (pM)	Found (pM)	RSD (%)	Recovery (%)
1	0.00	0.00	--	--
2	5.00	4.86	2.9	97.2
3	10.00	9.44	3.8	94.4
4	50.00	55.80	4.7	111.6
5	100.00	97.24	6.2	97.24

^a 10 folds diluted healthy human serum samples.

S2.12 Detection of miRNA-221 in cancer Cells

To investigate the feasibility of this PEC biosensor for the determination of miRNA-221 levels in real cell samples, HeLa cells and HEK293T cells lysate samples have been detected using this strategy, respectively. **Table S3** shows that this PEC biosensor has the feasibility and accuracy for real cell sample analysis.

Table S3 Results of determination of miRNA-221 in HeLa cells and HEK293T cells.

Sample ^a	This method (pM)	Control method (pM) ¹²	F-value ²³
1	3.67	3.66	4.04
2	3.42	3.45	3.92
3	3.58	3.57	3.85
4	0.56	0.55	4.57
5	0.63	0.63	4.21
6	0.59	0.58	4.32

^a 1, 2, 3: HEK293T cells; 4, 5, 6: HeLa cells

S2.13 Performance of control experimental

In the control experimental (Method A), WSe₂ was modified onto AuNPs/GE and thiolated-H2 was labelled with Cys and DA. A PEC biosensor was established with this DNA probe to detect miRNA-221. **Fig. S7 (A)** depicted the photocurrent increased with increasing miRNA concentration. As shown in **Fig. S7 (B)**, the photocurrent was proportional to the logarithm of the miRNA concentration in a linear range of 10.0 fM - 1.0 nM, with the linear regression equation of $I = 184.81 \log C(M) + 2964.71$ ($R^2 = 0.998$). The detection limit was 3.3 fM (S/N = 3). At the same concentration of 1 nM, the signal-to noise of Method A and this biosensor were 4.3 and 35.8, respectively. The present biosensor of Method A showed narrower linear response range and higher LOD than the biosensor we specially designed for the detection of miRNA-221.

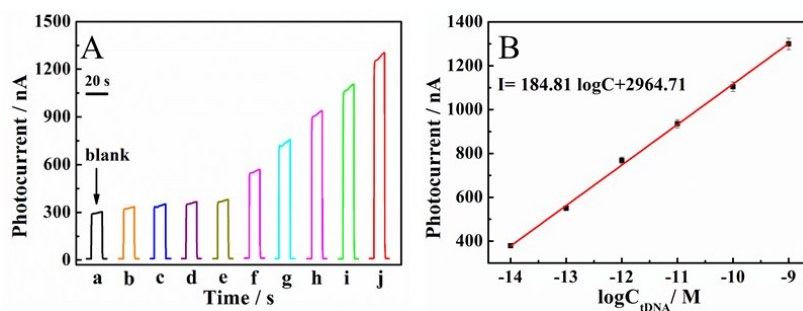
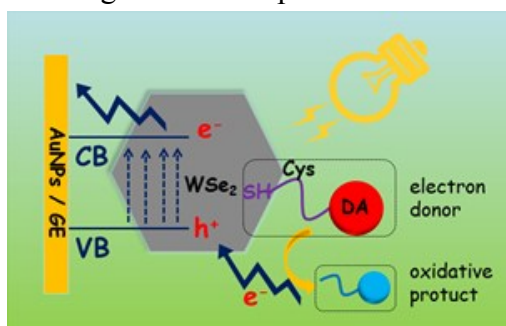


Fig. S7 (A) Photocurrent response of the biosensor to different concentrations of miRNA in phosphate buffer. The concentrations of miRNA were 0.0 aM, 10.0 fM, 100.0 fM, 1.0 pM, 10.0 pM, 100.0 pM and 1.0 nM (from a to j). (B) The linear calibration plot for the detection of different concentrations of miRNA with Method A.

S2.14 The mechanism of photocurrent generation

The proposed photocurrent-transducer mechanism was illustrated in **Schematic S2**. Under a visible-light illumination, WSe_2 absorb photons with energies higher than that of their band gaps, electrons are excited from the occupied valence band (VB) to the empty conduction band (CB), thus forming electron-hole pairs. As soon as the charge separation occurs, the electron-hole (e-h) pairs would be destined for recombination or charge transfer. The presence of an efficient electron donor, DA and Cys, would inhibit the e-h recombination. The VB holes would transfer to the surface of WSe_2 and then be neutralized by the electrons supplied by DA and Cys in the solution. Simultaneously, permitting the transfer of the CB electrons to the electrode to give rise to photocurrent, result in e-h pairs with sufficient long life and hence facilitate the generation of a high and stable photocurrent.



Schematic S2 Schematic illustration of the photocurrent generation mechanism.

References

1. X. Yu, M. S. Prévot, N. Guijarro and K. Sivula, *Nat Commun*, 2015, **6**, 7596.
2. X. Yu, M. S. Prévot and K. Sivula, *Chem. Mater.*, 2014, **26**, 5892-5899.
3. N. Dhenadhayalan, T.-W. Lin, H.-L. Lee and K.-C. Lin, *ACS Applied Nano Materials*, 2018, **1**, 3453-3463.
4. X. Chen and A. R. McDonald, *Adv Mater*, 2016, **28**, 5738-5746.
5. E. P. Nguyen, B. J. Carey, J. Z. Ou, J. van Embden, E. D. Gaspera, A. F. Chrimes, M. J. S. Spencer, S. Zhuiykov, K. Kalantar-Zadeh and T. Daeneke, *Adv Mater*, 2015, **27**, 6225-6229.
6. L.-S. Jang and H.-K. Keng, *Biomed Microdevices*, 2008, **10**, 203-211.
7. C. Ye, M. Q. Wang, Z. F. Gao, Y. Zhang, J. L. Lei, H. Q. Luo and N. B. Li, *Anal Chem*, 2016, **88**, 11444-11449.
8. H. Y. Lau, H. Wu, E. J. H. Wee, M. Trau, Y. Wang and J. R. Botella, *Sci. Rep-UK*, 2017, **7**, 38896.
9. L. Bettanin, S. Saba, F. Z. Galetto, G. A. Mike, J. Rafique and A. L. Braga, *Tetrahedron Letters*, 2017, **58**, 4713-4716.
10. H. V. Tran, B. Piro, S. Reisberg, L. D. Tran, H. T. Duc and M. C. Pham, *Biosens Bioelectron*, 2013, **49**, 164-169.
11. Y. Qi, X. Lu, Q. Feng, W. Fan, C. Liu and Z. Li, *ACS Sensors*, 2018, **3**, 2667-2674.
12. J. Hu, M.-h. Liu and C.-y. Zhang, *Chem. Sci.*, 2018, **9**, 4258-4267.
13. J. T. Han, J. I. Jang, H. Kim, J. Y. Hwang, H. K. Yoo, J. S. Woo, S. Choi, H. Y. Kim, H. J. Jeong, S. Y. Jeong, K.-J. Baeg, K. Cho and G.-W. Lee, *Sci Rep*, 2014, **4**, 5133.
14. S. S. Chou, M. De, J. Kim, S. Byun, C. Dykstra, J. Yu, J. Huang and V. P. Dravid, *JACS*, 2013, **135**, 4584-4587.
15. X. Yu, N. Guijarro, M. Johnson and K. Sivula, *Nano Letters*, 2018, **18**, 215-222.
16. J.-S. Kim, H.-W. Yoo, H. O. Choi and H.-T. Jung, *Nano Lett.*, 2014, **14**, 5941-5947.
17. Z. Yu, Y. Pan, Y. Shen, Z. Wang, Z.-Y. Ong, T. Xu, R. Xin, L. Pan, B. Wang, L. Sun, J. Wang, G. Zhang, Y. W. Zhang, Y. Shi and X. Wang, *Nat Commun*, 2014, **5**, 5290.
18. X.-M. Shi, G.-C. Fan, Q. Shen and J.-J. Zhu, *ACS Appl. Mater. Inter.*, 2016, **8**, 35091-35098.
19. Q. Shen, X. Shi, M. Fan, L. Han, L. Wang and Q. Fan, *J Electroanal Chem*, 2015, **759**, 61-66.
20. R. Thota and V. Ganesh, *RSC Advances*, 2016, **6**, 49578-49587.
21. J. Tang, Z. Shi, R. M. Berry and K. C. Tam, *Ind Eng Chem Res*, 2015, **54**, 3299-3308.
22. Y. Bai, B. Zhang, L. Chen, Z. Lin, X. Zhang, D. Ge, W. Shi and Y. Sun, *Nanoscale Res Lett*, 2018, **13**, 287.
23. S. J. Haswell, *Statistics for analytical chemistry, 3rd edition*, 1994.